YTUP

Journal of Thermal Engineering
https://jten.yildiz.edu.tr/
https://doi.org/10.47481/jten.0015

RESEARCH ARTICLE

Fin geometry and pitch length optimization for forced convection in tubes: a numerical study

Ahmet Furkan Urkut[1,*], Mehmed Rafet Özdemir[2]

[1]Faculty of Engineering, Marmara University, Istanbul, 34854, Türkiye
[2]Faculty of Engineering, Marmara University, Istanbul, 34854, Türkiye

Abstract

Many applications require smaller, faster, and more powerful electronic devices, leading to excess heat that needs to be removed from the system. Micro-finned tubes are a preferred method to increase the heat-transfer performance of cooling systems. There are a limited number of studies on the fin geometry of micro-finned tubes with respect to thermohydraulic performance and entropy-generation analysis, especially for diameters under 10 mm. To address this literature gap, this study numerically investigates the entropy generation rates and thermohydraulic performance of 8-mm-diameter horizontal tubes with square, circular, and triangular fins compared with those of a smooth tube. In this regard, numerical studies were conducted at constant heat flux with Reynolds numbers ranging from 400 to 2000 in the laminar regime and from 5000 to 9000 in the turbulent regime, using computational fluid dynamics. The Nusselt number increased by 140%, 218%, and 180% for the square, circular, and triangular finned tubes, respectively, compared with the smooth tube in the laminar flow regime. In the turbulent region, the Nusselt number increased by 3.4%, 29%, and 7.5% for the square, circular, and triangular finned tubes, respectively. Since the tube with circular-fin geometry demonstrated the greatest heat-transfer capability in both laminar and turbulent regimes, numerical analyses were conducted on circular-fin tube models with pitch lengths of 3-6 mm to enhance heat-transfer performance. The device with a 3-mm pitch length demonstrated greater thermohydraulic performance despite having slightly higher entropy generation rate and friction factor than the other versions. The findings of this study offer valuable insights to inform the design of more efficient thermal systems.

Keywords: Thermohydraulic analysis, entropy generation rate, fin geometry optimization

Cite this article as: Urkut, A. F., & Özdemir, M. R. (2026). Fin geometry and pitch length optimization for forced convection in tubes: A numerical study. Journal of Thermal Engineering, 12(3), 2–14. https://doi.org/10.47481/jten.0015

1. Introduction

The development of technology and a growing population have led to an increased demand for high-performance electronic devices. Today, most operations require electronic devices that are faster, smaller, more reliable, and more powerful. However, these requirements also lead to elevated heat fluxes that need to be dissipated to prevent failures. Thus, the design and development of effective cooling schemes are critical for the temperature control [1-3]. Various thermal management solutions have been proposed for electronic devices in the literature, such as spray cooling, forced liquid cooling, immersion cooling, and flow boiling. These mechanisms have been widely used in electronic systems, solar systems and battery cooling systems [4]. All of those techniques have both advantages and drawbacks. Flow boiling heat transfer (HT) can yield higher HT with less pumping power than in the single-phase HT mode. But it is a complicated process and underlying physical phenomena behind it are still not clearly understood [5, 6]. Although the spray cooling HT can provide high HT rates, the accompanying high pressure drop and small spray nozzles are drawbacks. The small sized flow paths may lead to clogging unless they provide similar spray patterns [7]. The immersion-cooling HT has great potential for cooling performance. But the system's complexity, expense, dielectric fluid evaporation, and added weight render it impracticable [8]. Still, most researchers and technology provider companies prefer single-phase HT methods since the theory is well-established predictable, controllable and cheap [9, 10].

*Corresponding Author
E-mail Adress: furkan.urkut@marmara.edu.tr

Submitted: 19 December 2025; **Accepted:** 11 January 2026

This paper was recommended for publication in revised form by Editorin-Chief Ahmet Selim Dalkılıç

The choice of refrigerants in cooling systems is dependent on thermodynamic, safety and technical aspects [11].Conventional refrigerants, such as chlorofluorocarbons (CFCs) and hydrochlorofluorocarbons (HCFCs), were widely used because of their excellent cooling performance. Nevertheless, increasing pollution and environmental concerns have led to the universal banning of most of these type refrigerants [12, 13]. Synthetic refrigerants can stay in the atmosphere for many years and can cause significant harm to life on the earth [14]. Therefore, natural refrigerants like water and CO_2 have attracted attention from the researchers. Even though there are various natural refrigerants, they cannot satisfy the necessary specifications [12]. For instance, ammonia is flammable and toxic, therefore, not appropriate for some cases [15]. Also, there are notable concerns regarding the employment of hydrocarbons as a refrigerant due to their flammability [14]. On the other hand, water has no risk of future limitations regarding coolant environmental impact [16]. Water is one of the earliest environmentally friendly natural refrigerants employed in cooling operations due to its ease of availability and favourable thermodynamics and chemical properties [17]. Compared with other refrigerants, water's high critical point makes it a salient coolant in heat pump applications [16]. But, the employment of water as a coolant is limited to applications where the cooling requirements are above the freezing point of water [16]. Therefore, some cooling applications may require the addition of antifreeze additives to the water.

The finned pipes are employed to increase the HT performance of those cooling systems by creating local turbulence in the flow , thus promoting mixing, and by increasing the HT surface area. There are various studies [18-32] in the literature that indicate finned tubes significantly enhance the HT performance for different refrigerants. However, discrepancies remain regarding which fin shape is most favorable with respect to pressure loss and HT performance. Several studies in the literature investigate the effect of tube groove geometry on HT performance. Bilen et al. [18] experimentally investigated the HT performance of 36 mm inner diameter horizontal tubes that have different groove shapes. Their results indicated that the circular corrugated tube had the largest HT enhancement, while the rectangular corrugated tube had the smallest HT augmentation. The results of Ramadhan et al. [24] demonstrated that triangular finned tube gives the highest performance evaluation criteria. Kaood et al. [28] investigated the thermohydraulic performance 10 mm diameter grooved pipes. Their findings indicated that curved and triangular groove shapes exhibited superior thermal-hydraulic performance compared with other geometries. On the other hand, the results of Selvaraj et al. [23] indicated that trapezoidal finned tube has greatest thermohydraulic performance while square finned tube shows the lowest thermohydraulic performance. A trade-off between HT augmentation and pressure loss must be optimized. A current literature review of HT and pressure-drop characteristics of horizontal single-phase flow inside micro-fin tubes for water and other working fluids is presented in Table 1 to show the state of the art in this field. Although numerous studies have investigated various enhanced heat transfer methods, research focusing on how micro-fin geometry affects the thermohydraulic behavior of micro-finned tubes remains limited. Few studies examine the fin geometry of micro-finned tubes with respect to entropy generation analysis and performance evaluation criteria (PEC), especially for tube diameters smaller than 10 mm. In the present study, to address this gap in the literature, PEC, entropy generation, HT, and pressure-drop characteristics of water inside an 8 mm diameter horizontal finned tube with different fin shapes and pitch lengths were analysed numerically and compared with those of a tube having no fin using computational fluid dynamics (CFD). Moreover, it aims to identify the optimized fin shape and pitch length that have superior thermohydraulic characteristics. Thus, this study aims to contribute to the development of more efficient thermal management and cooling systems by improving understanding of the effects of micro-fin geometry on thermohydraulic performance.

Subsequent sections of this paper outline the methodology, including the geometry of the models, boundary conditions, mathematical modeling, meshing, and the solution procedure, and then present the results and discussion.

Table 1. Summary of studies on single phase thermohydraulic characteristics of water and some other refrigerants inside finned tubes

References	Working Fluid	Diameter	Conditions	Results
Bilen et al. [18]	Air	36 mm	Re numbers ranges from 10000 to 38000, under constant power of 180 W.	The HT performance is enhanced up to and 47% for rectangular corrugated, 58% for trapezoidal corrugated and 63% for circular corrugated tube.
Selvaraj et al. [19]	Water-ethylene glycol mixture	38.14 mm	For Re numbers between 4900 and 13300, under constant power of 1000 W.	HT augmentation is achieved up to 55% for square corrugated tube, 36% for circular corrugated tube and 10% for trapezoidal corrugated tube compared to the smooth tube.
Pethkool et al. [20]	Water	24.5, 25 and 25.5 mm	Re number varying from 5500 to 60000	HT was enhanced up to 123% to 232% compared to the plain tube. Friction factor of the finned tube is 1.46 to 1.93 times over the plain tube.
Inoue & Ichinose [21]	Water	4 mm	Heat flux varied from 2.09kW/m^2 to 84.1kW/m^2.	Finned tube has higher Nu number and friction factor comparing the plain tube in turbulent flow region. Maximum HT coefficients obtained at the helix angle about 15°.

Celen et al. [22]	Water	7.48 mm	Re number ranging from 5725 to 25353	Friction factor values of the micro finned tube were larger than those of the plain tube.
Selvaraj et al. [23]	Water	38.14 mm	For Re numbers between 5000 and 13500 and 9.6996 kW/m^2 constant heat flux.	Trapezoidal finned tube has greatest thermohydraulic performance and square finned tube gives the smallest enhancement in thermohydraulic performance compared to the smooth tube.
Ramadhan et al. [24]	Air	50 mm	For Re numbers between 10000 and 2000 and under 1 kW/m^2 constant heat flux	The finned tube notably increases the HT at about 64.4 % over the smooth tube and triangular finned tube gives the highest performance evaluation criteria compared to the other finned tubes.
Aroonrat et al. [25]	Water	7.1 mm	Re number changing from 4000 to 10000 and under heat flux of 3.5 kW/m^2	Helical finned tubes have larger values of friction factor and Nu number than those of the plain tube. The thermal enhancement factor of the finned tubes is nearly 1.4 to 2.2 for a pitch length of 12.7 mm; 1.1 to 1.3 for pitch lengths of 203, 254, and 305 mm, respectively.
Mohammed et al. [26]	Water	10 mm	Re number ranging between 5000 and 60000 and under heat flux of 500 kW/m^2	Increasing of the fin height, fin width and Re number improves the Nu number. The largest Nu number was achieved with fin height to pipe diameter ratio of 0.1.
Wang et al. [27]	Aqueous ethylene glycol	22.48 mm	Re number varying from 5000 to 34000 and heat flux of 26 - 46 kW/m^2	Helically finned tube augmented the j factor nearly 3.5 times compared to the smooth tube.
Kaood et al. [28]	Water	10 mm	For Re numbers ranging between 5000 and 61000 and constant heat flux of 500 kW/m^2	Both inward and outward triangular and curved fin shapes have the greater thermohydraulic performance than rectangular and trapezoidal fins.
Mogaji et al. [29]	Water	19 mm	For Re numbers between 12000 and 22000, at constant wall temperature of 350 K	Nu number enhancements were achieved as 125% while, friction factor penalties were obtained as 531% compared to the plain tube.

2. Methodology

2.1. Geometry of the models

Three types of fin shapes (circular, triangular and square) were modeled to examine the influences of fin shape on HT performance, pressure drop, friction factor and entropy generation rate in single-phase water flow. Analyses were performed using 2-D model of smooth and finned tubes having 8 mm diameter and 1 m length. Fig. 1 presents a schematic diagram of the geometric shapes of the finned tube models, where p_l denotes the pitch length. For all finned tube models, pitch length and the number of fins were set to 4 mm and 235 respectively. For the circular fins, semi-circular protrusions with a diameter of 1 mm were employed. Square and triangular fins are generated from square and equilateral triangular protrusions with a side length of 1 mm. The first fin was placed at the distance of 30 mm from the entrance of the tube. Besides, circular finned tube models of various pitch lengths (3, 4, 5 and 6 mm) were created to examine the impact of pitch length on thermohydraulic characteristics.

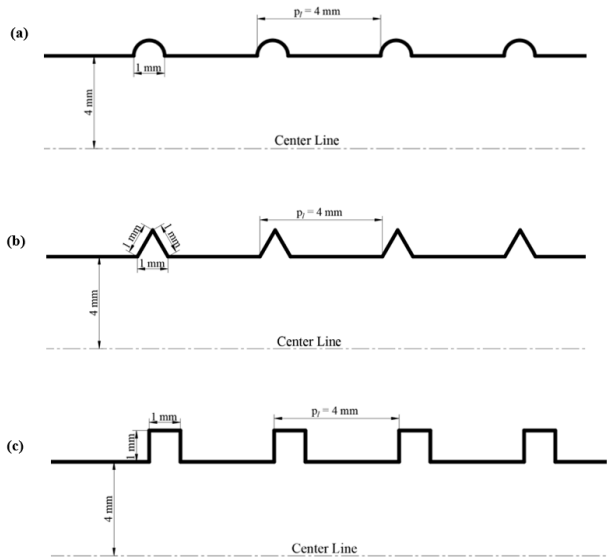

Figure 1. Schematic diagram of finned tubes, **(a)** circular fin, **(b)** triangular fin and **(c)** square fin

2.2. Boundary conditions

In turbulent flow, constant uniform heat flux of 40 kW/m^2 was imposed on wall of the tube and inlet temperature was set to 20 °C. Analyses were run for Re number 5000 to 9000 for turbulent flow. For laminar flow, constant uniform heat flux of 3.5 kW/m^2 was implemented on wall of the tube and inlet temperature of the working fluid was set to 5 °C. A higher constant heat flux was applied in the turbulent flow case to achieve a meaningful temperature difference between the inlet and outlet of the pipe. Analyses were run for the Re numbers varying from 400 to 2000. Boundary conditions imposed on the 2-D axisymmetric model. Pressure outlet boundary condition (atmospheric pressure) was defined at the outlet of the tube.

2.3. Mathematical modeling

For the governing equations of the flow field, steady, 2-D continuity equation, incompressible Reynolds-averaged Navier-Stokes(RANS) equations and the energy equation were used. The governing equations [33, 34] are shown below.

Continuity equation:

$$\frac{\partial (\rho u_i)}{\partial x_i} = 0 \quad (1)$$

Momentum equation:

$$\frac{\partial (\rho u_i u_j)}{\partial x_j} = -\frac{\partial P}{\partial x_i} + \frac{\partial}{\partial x_j}\left[\mu\left(\frac{\partial u_i}{\partial x_j} + \frac{\partial u_j}{\partial x_i}\right)\right] + \frac{\partial}{\partial x_j}(-\rho\overline{u_i' u_j'}) \quad (2)$$

Energy equation:

$$\nabla\left[\vec{u}(\rho E + p)\right] = \nabla\left[k_{eff}\nabla T + \left(\overline{\overline{\tau}}_{eff}\vec{u}\right)\right] \quad (3)$$

Where k_{eff} refers to effective conductivity, E denotes the total energy, p refers to pressure, τ_{eff} denotes stress tensor, signifies the mean velocity and u' signifies fluctuated velocity component. Standard k-ω model, k-ε model and Shear-Stress Transport (SST) k-ω model are the most commonly used turbulence models [35, 36]. Menter [37], developed the SST k-ω model in an effort to proficiently mix the accurate and well-established method of the k-ω model in the regions nearby the wall with the free flow independence of the k-ε model in the regions far from the wall. The SST k-ω model more precise and dependable for a broader group of flows compared to the standard k-ω model [33]. In this study, SST k-ω model is employed as turbulence model. Transport equations of the SST k-ω model are presented in equations (4) and (5) [33].

$$\frac{\partial}{\partial x_i}(\rho k u_i) = \frac{\partial}{\partial x_j}\left(\Gamma_k \frac{\partial k}{\partial x_j}\right) + \widetilde{G_k} - Y_k + S_k \quad (4)$$

$$\frac{\partial}{\partial x_j}(\rho \omega u_j) = \frac{\partial}{\partial x_j}\left(\Gamma_\omega \frac{\partial k}{\partial x_j}\right) + G_\omega - Y_\omega + D_\omega + S_\omega \quad (5)$$

Where k, ω D_ω and refer to the turbulence kinetic energy, specific dissipation rate and the cross-diffusion term respectively. $\widetilde{G_k}$ refers to the generation of turbulence kinetic energy due to the mean velocity gradients.Y_k and Y_ω refer to the dissipation of k and ω because of the turbulence and S_k and S_ω denote user-defined source terms. Γ_k and Γ_ω signify the effective diffusivity of k and ω, respectively and they are defined below.

$$\Gamma_k = \mu + \frac{\mu_t}{\sigma_k} \quad (6)$$

$$\Gamma_\omega = \mu + \frac{\mu_t}{\sigma_\omega} \quad (7)$$

Where σ_k and σ_ω refer to the turbulent Prandtl number for k and ω, in turn, and μ_t denotes the turbulent viscosity.

2.4. Meshing

For smooth tube model, structured rectangular mesh generated using 24000 mesh elements. Value of the y+ for cells adjacent to the wall of the tube was controlled and reported as 1.032 which is an acceptable value for near wall mesh resolution. Further information can be found in ref. [38]. Quadrilateral mesh was generated for each finned tube models. Grid structure of the square, circular and triangular finned tube models are shown in Fig. 2. Value of the y + for cells adjacent to the wall of the tube computed as 0.08, 0.054 and 0.066 for circular, square and triangular finned tube models respectively. These y + values are quite agreeable regarding their recommended values for the models [33]. To confirm that the numerical results were mesh independent, all the finned tube models were run employing different number of mesh elements. Nu number and wall temperature of the tubes reported as a result of the analysis using different number of mesh elements at Re number of 7000 for circular, square and triangular finned tubes and shown in Tables 2, 3, and 4, respectively.

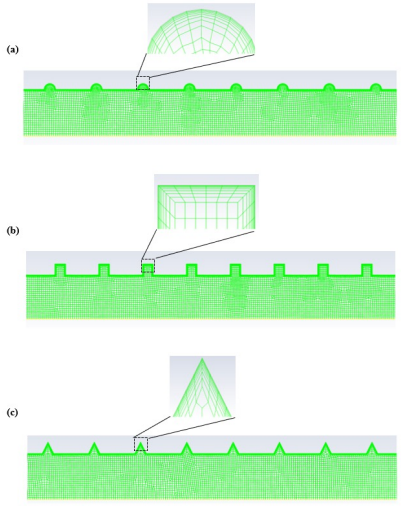

Figure 2. Grid structure of the **(a)** circular finned tube, **(b)** square finned tube and **(c)** triangular finned tube

Table 2. Mesh independence results for circular finned tube at Reynolds number of 7000

Number of Elements	Wall Temperature (K)	Nu Number
269030	304.3	81.45
223140	304.3	81.45
205655	304.3	81.45
167700	304.1	83.48
133860	304.1	83.48

Table 3. Mesh independence results for square finned tube at Reynolds number of 7000

Number of Elements	Wall Temperature (K)	Nu Number
235260	311.1	64.1
219235	311.1	64.1
207210	311.1	64.1
181920	310.2	68.32
129950	309.3	73.41

Table 4. Mesh independence results for triangular finned tube at Reynolds number of 7000

Number of Elements	Wall Temperature (K)	Nu Number
214880	306.9	68.9
205590	306.9	68.9
190810	306.9	68.9
173320	306.4	72.8
117090	305.6	79.5

2.5. Solution Procedure

The governing equations were computed by using the commercial CFD program ANSYS Fluent 2021 R1. A control volume-based technique involves integrating the transport equation around each control volume and produces a control volume based discrete equation that depicts the conservation law [33]. Pressure based type of solver was employed with coupled algorithm. To obtain higher-order accuracy, second-order upwind scheme was selected for discretization. Axisymmetric 2-D model was used for the simulations in an effort to reduce the computation time. SST k-ω turbulence model was selected for the turbulent region as mentioned above. SST k-ω and k-ω models can also give good results for laminar to turbulent transition flows in low Re number regions [39, 40]. For the finned tube models SST *k*- turbulence model also employed in laminar region since fins promote laminar to turbulent transition throughout the flow. Nu number, friction factor and pressure drop of water flow through horizontal smooth and finned tubes were investigated in both laminar and turbulent regions. Besides, PEC and entropy generation rates of the models were computed in order to provide more eligible comparison of thermohydraulic performance of the tubes. Expression for pressure drop ΔP, is shown below.

$$\Delta P = f\frac{L}{D}\frac{\rho u^2}{2} \tag{8}$$

Where, f is friction factor, D is the diameter of the tube and L is the length of the tube. Expression for Re number is given as follow:

$$Re = \frac{\rho u D_h}{\mu} = \frac{u D_h}{v} \tag{9}$$

Where ρ is the density, D_h is the hydraulic diameter, μ is the dynamic viscosity and v is the kinematic viscosity. Expression for the Nu number is shown below.

$$Nu = \frac{hD_h}{k_f} \tag{10}$$

Where h is the HT coefficient and k_f is the thermal conductivity of the fluid. Taking into account both Nu number and friction factor, Performance Evaluation Criteria(PEC)provides eligible comparison between systems. Correlation for PEC is presented in Equation(11) [41, 42].

$$PEC = \frac{(Nu/Nu_s)}{(f/f_s)^{1/3}} \tag{11}$$

Where Nu_s is the Nu number of the smooth tube and f_s is the friction factor of the smooth tube. Correlation for the entropy generation per unit length is presented below [43].

$$\dot{S}'_{gen} = \frac{q'^2}{\pi k T^2 Nu\,(Re, Pr)} + \frac{32\dot{m}^3}{\pi^2 \rho^2 T}\frac{f(Re)}{D^5} \tag{12}$$

Where q' is the HT rate per unit length, $\dot{m}$ is the mass flow rate and T is the temperature. Numerical results of the study were validated with some well-established correlations from the literature. In laminar region, developing laminar flow correlations were used since the flow is developing in laminar region. To validate the numerical results for Nu number for developing laminar flow, Equation (13) [44] and Equation(15)[45] were used from Shah and London [46].

$$Nu = 1.953\,(x^*)^{-1/3} \quad \text{for} \le 0.003$$

$$Nu = 4.364 + 0.0722/x^* \quad \text{for} > 0.003 \tag{13}$$

$$x^* = \frac{x}{D_h Re Pr} \tag{14}$$

Where x^* denotes the dimensionless axial distance and x denotes the cartesian coordinate along the flow direction.

$$Nu = 0.775\,(f_f Re)^{1/3}(x^*)^{-1/3} \tag{15}$$

Where f_f refers to the fanning friction factor for fully developed flow. For validating the numerical results for friction factor in developing laminar flow region Equation(16) [45] is used from Shah and London [46].

$$f_{app}\,Re = 3.44\,(x^+)^{-0.5} + \frac{K(\infty)/4\,(x^+) + fRe - 3.44\,(x^+)^{-0.5}}{1 + 0.00021\,(x^+)^{-0.2}} \quad (16)$$

$$x^+ = \frac{x}{D_h Re} \quad (17)$$

Where, $K(\infty)$ is the incremental pressure drop number, f_{app} is the apparent friction factor and x^+ is the dimensionless axial distance. For validating the numerical results for Nu number in turbulent region, Dittus-Boelter [47], Gnielinski [48] and second Petukhov correlations were used. The Dittus-Boelter equation [46] for Nu number in turbulent flow is presented in Equation (18).

$$Nu = 0.023 \cdot Re^{0.8} \cdot Pr^{0.4} \quad (18)$$

The correlation proposed by Gnielinski [48] for Nu number is shown below.

$$Nu = \frac{\left(\frac{f}{8}\right)(Re - 1000)\,Pr}{1 + 12.7\left(\frac{f}{8}\right)^{0.5}(Pr^{2/3} - 1)} \quad (19)$$

Another correlation known as second Petukhov equation for Nu number in turbulent flow is presented below [6].

$$Nu = \frac{\left(\frac{f}{8}\right)RePr}{1.07 + 12.7\left(\frac{f}{8}\right)^{0.5}(Pr^{2/3} - 1)} \quad (20)$$

Correlation for Darcy friction factor proposed by Blasius [49] presented below.

$$f = 0.316\,Re^{-\frac{1}{4}} \quad (21)$$

3. Results and discussion

3.1. Validation of the numerical model

Numerical results for laminar and turbulent water flow in horizontal smooth tube were compared with well-established correlations in the literature. Comparison of the CFD results and correlations are presented in Fig. 3.

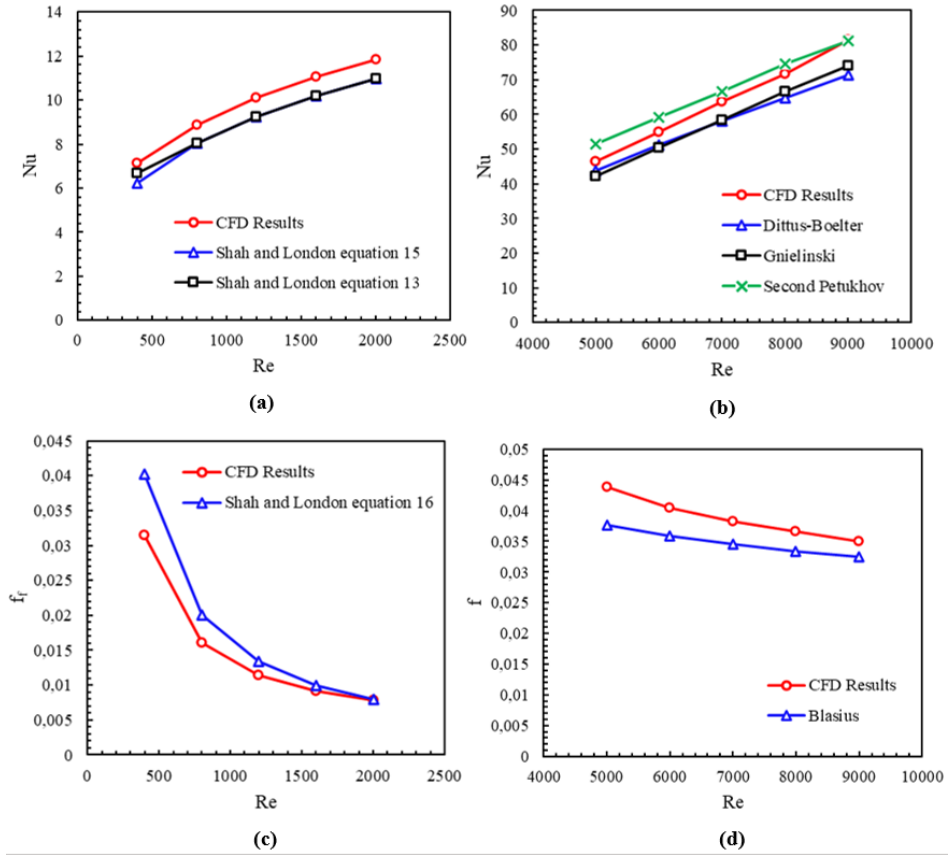

Figure 3. Validation of the results for Nusselt number **(a)** in laminar region **(b)** in turbulent region; validation of the results for **(c)** friction factor in laminar region **(d)** friction factor in turbulent region

In the laminar region, the mean absolute error(MAE)of the Nu number ranges from 6.43% to 10.36% for Equation(13)and from 8.21% to 14.53% for Equation(15),whereas the MAE of the friction factor ranges from 2.5% to 21.89% for the correlation given in Equation(16).For the turbulent flow, MAE of the Nu number ranges from 6.02% to 13.88%, 7.45% to 10.2% and 0.025% to 9.93% for Dittus-Boelter [47], Gnielinski [48] and second Petukhov correlations respectively. MAE of the friction factor ranges from 7.32% to 16.55% for the Blasius [49] correlation. Considering these values, it was concluded that the results were consistent with the literature, confirming the validity of the model.

3.2. Finned tube models

The impacts of fin shape on HT, friction factor and pressure loss characteristics were numerically investigated and compared with those of the smooth tube. PEC values and entropy generation rates of each finned tube model was calculated. It should be taken into consideration that flow in the laminar region is a developing flow. Fig. 4 shows the Nu number for finned and smooth tubes in turbulent and laminar regions. It was seen that in laminar region, Nu number increases up to 140%, 218% and 180% for square, circular and triangular finned tube respectively compared to the tube with no fin. In turbulent region, Nu number increases up to 3.4%, 29% and 7.5% for square, circular and triangular finned tube respectively compared to smooth tube. Results indicated that circular finned tube has 1.16 to 3.18 and 1.2 to 1.3 times higher Nu numbers compared to those of the smooth tube in laminar and turbulent regions respectively. Square finned tube has the lowest Nu numbers among all the finned tube models.

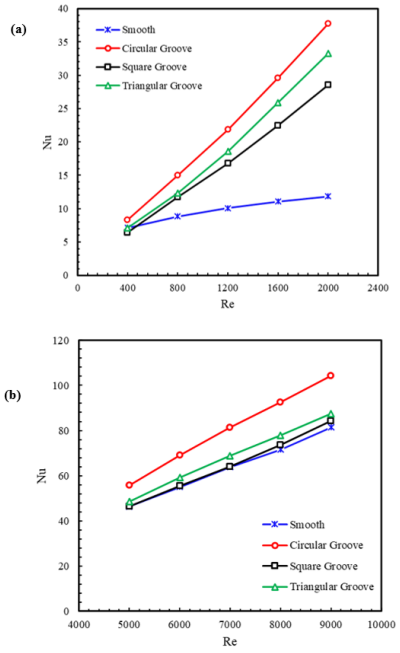

Figure 4. Reynolds number versus Nusselt number plot of finned and smooth tubes for **(a)** laminar and **(b)** turbulent regions

In this study, it was observed that the Nu number increased by up to 29% for the circular finned tube compared to the smooth tube, for Re numbers ranging from 5000 to 9000. This finding is consistent with the results reported in the literature. Selveraj et al. [23] performed the tests for Re number varying from 5000 to 13500 using water inside finned tubes and reported that the Nu number enhanced by up to 37% for the circular finned tube compared to the smooth tube. In their study, it was also observed that the square finned tube exhibited the lowest enhancement in the Nu number. Kaood et al. [28] studied the thermohydraulic aspects of water inside 10 mm diameter transverse corrugated tube and reported that outward rectangular corrugation shape has the smallest Nu number enhancement compared to smooth tube among the other corrugation shapes. Bilen et al. [18] experimentally investigated the HT performance of 36 mm inner diameter horizontal tubes that have different groove shapes. Their results also indicated that circular corrugated tube has the largest HT enhancement while, rectangular corrugated tube has the minimum HT augmentation.

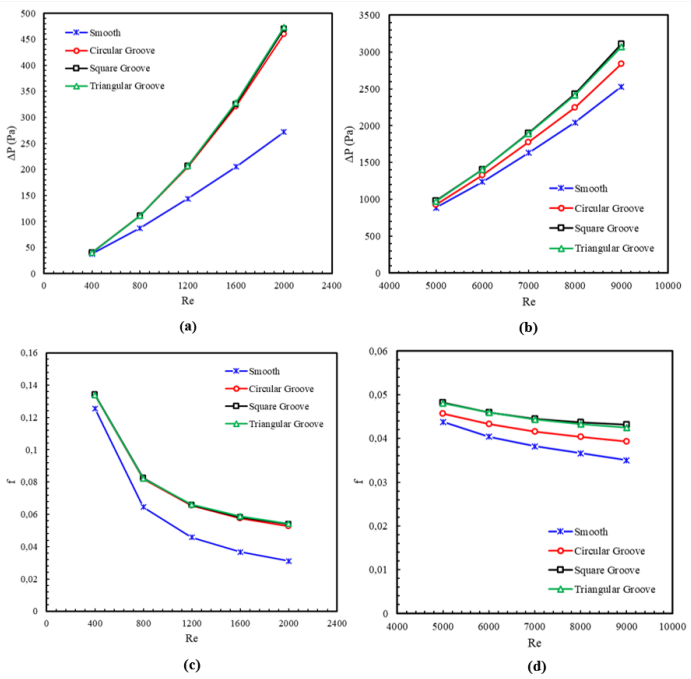

Figure 5. Reynolds number versus pressure drop plot of finned and smooth tubes for **(a)** laminar and **(b)** turbulent regions; Reynolds number versus friction factor plot of finned and smooth tubes for **(c)** laminar and **(d)** turbulent flow

In Fig. 5 pressure drop and friction factor values of finned and smooth tubes in laminar and turbulent regions are presented. As can be observed from Fig. 5, finned tubes have very similar pressure drop values in the laminar region while, circular finned tube has slightly lower pressure drop compared to square and triangular finned tubes in the turbulent region. As expected, smooth tube has the lowest friction factor in both laminar and turbulent regions. The findings revealed that the finned tubes have almost the same friction factor values in the laminar zone. Note that in laminar region

friction factor is independent of the roughness of the tube surface [6]. It was found that, in the laminar flow region, the finned tubes exhibit friction factors that are on average 6.6% to 71.5% higher than those of the smooth tube. The results showed that, in the turbulent flow region, the friction factors were 10–23.1%, 4.3–12.3%, and 9.8–21.4% higher for the square, circular, and triangular finned tubes, respectively, compared to those of the smooth tube. It was observed that square finned tube has friction factor values slightly higher than triangular finned tube and circular finned tube has lower friction factor values compared to square and triangular finned tubes in turbulent region. Square fins possess larger area for recirculation inside the fins. This larger recirculation area inside the square fins give rise to higher pressure loss and thus larger friction factor values. Hence, owing to its geometry square finned tube cause larger friction factor and pressure drop values compared to circular fins in turbulent region.

Kaood et al. [28] also investigated the friction factor of various corrugation shapes for Re number changing from 5000 to 61000 for horizontal water flow inside the tubes. In their study, it was seen that rectangular corrugation shape has the highest friction factor compared to trapezoidal, curved, and triangular corrugation shapes. They reported that mean friction factor of the rectangular corrugation shape is 162.27% larger than the plain tube. Besides, Ramadhan et al. [24] pointed out that for corrugation depth to pipe diameter ratio of 0.1, rectangular finned tube has the largest friction factor values among the finned tubes.

In Fig. 6 PEC values for finned tubes in laminar and turbulent regions are shown. Circular finned tube has higher PEC values among the finned tube models. Circular and triangular finned tubes have PEC values greater than 1 in both laminar and turbulent regions. On the other hand, square finned tube has PEC values lower than 1 in turbulent region. Findings indicated that, circular finned tube has superior thermohydraulic performance compared to square finned, triangular finned and smooth tube in both laminar and turbulent zones.

Fig. 7 presents the ratio of entropy generation rate of finned tubes, to entropy generation rate of smooth tube, for laminar and turbulent regions. It was seen that square finned tube has the largest entropy generation rate in both laminar and turbulent region. Ramadhan et al. [24] reported that rectangular fin gives the minimum efficiency values and possesses the highest entropy generation among all the finned tubes. It is substantial to consider the entropy generation resulting from the vortices that produced by fins because entropy generation tends to increase due to the recirculation within the corrugations. This present paper also revealed that square finned tube has lower HT and thermohydraulic performance and it has the highest entropy generation rate. Larger recirculation area inside square fins also give rise to larger entropy generation rates compared to circular and triangular fins. On the other hand, circular finned tube has the lowest entropy generation rate among all the finned tube models.

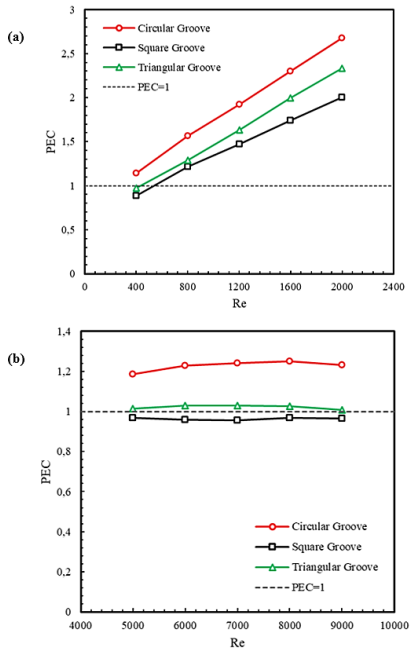

Figure 6. Reynolds number versus PEC plot of finned tubes for **(a)** laminar and **(b)** turbulent flow

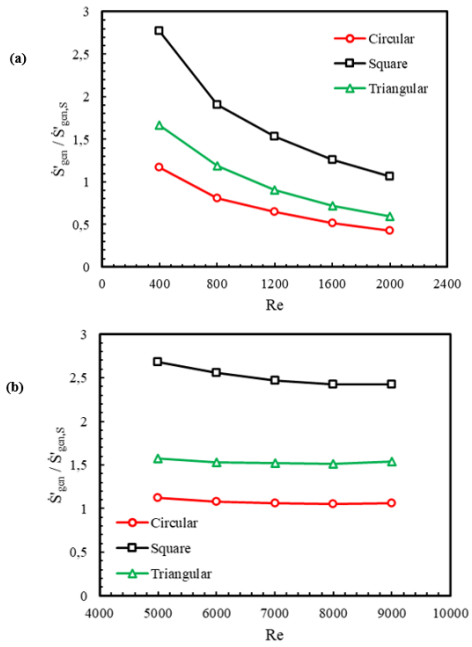

Figure 7. Reynolds number versus ratio of entropy generation rate of finned tubes to smooth tube plot for **(a)** laminar and **(b)**turbulent flow

To understand the flow structure better, velocity vectors contour plots of finned tubes are shown in Fig. 8 for laminar and turbulent regions. Since fins cause disturbance in the flow and promote fluid mixing, enhanced tubes have superior HT performance comparing the smooth tubes. The rise in the surface area because of the fins

also gives contribution to the improvement of the HT. Nevertheless, finned tubes have higher friction factor and pressure drop values compared to smooth tube. Disturbance and recirculation in the flow generated by fins result in larger friction factor and pressure loss values. Besides, it was observed that because of its geometry square fins has lower HT enhancement compared to circular and triangular fins. As demonstrated in Fig. 8, because of the sharp corners of the square fin, recirculation generated by the fin is trapped inside the fin, which prevents good fluid mixing and thus decreases the HT enhancement also causes rise in friction factor. Eventually, lower Nu numbers and larger friction factor values of square fins cause higher entropy generation. Circular fins provide greater surface sweep, thus recirculation and disturbances created by the fin further promote turbulence and fluid mixing, yielding higher HT enhancement. Another factor for the lower HT augmentation of square finned tube is the larger difference between wall temperature of the tube and bulk temperature of the working fluid. The increase in the difference among the wall temperature and the bulk temperature of the fluid weakens the HT, yielding a decline in the Nu number [50, 51]. Better fluid mixing provides smaller difference among the wall temperature and the bulk temperature of the fluid for circular and triangular finned tubes compared to square finned tube. Accordingly, with its lower Nu number and larger pressure loss values, square finned tube has lower PEC values and thus has lower thermohydraulic performance in comparison with circular and triangular finned tubes.

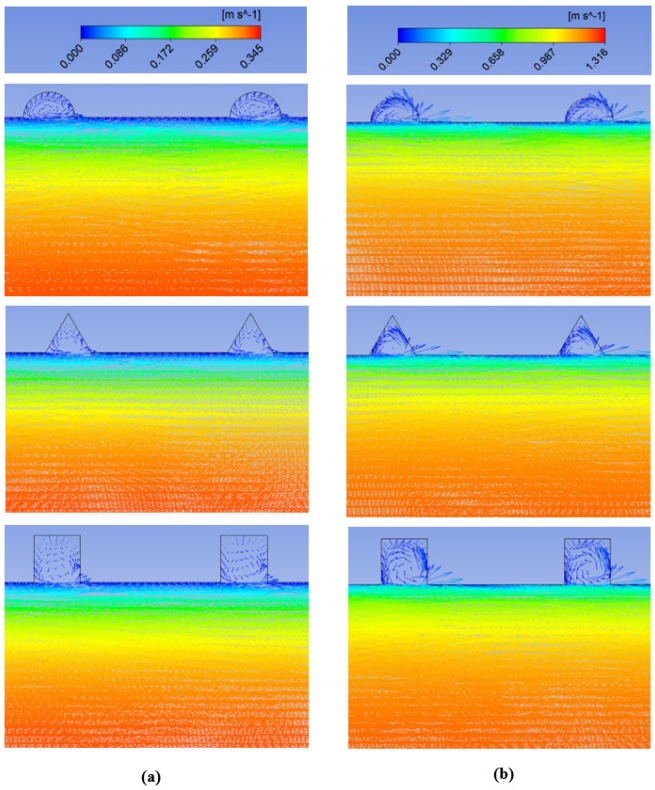

Figure 8. Velocity vector contours of the finned tubes for **(a)** Reynolds number of 1200 and **(b)** for Reynolds number of 8000

3.3. Analysis of the effects of pitch length in circular finned tube

With the intention of further enhance the HT performance of the circular finned tube, impacts of the pitch length on HT and pressure loss characteristics are studied numerically. In addition to the model with a 4 mm pitch length, additional numerical models with pitch lengths of 3, 5, and 6 mm were investigated for the circular finned tube. Fig. 9 depicts the Nu numbers of the circular finned tube models with different pitch lengths in laminar and turbulent regions. In laminar region model with 3 mm pitch length has slightly higher Nu numbers than the other models. Models with 4, 5 and 6 mm pitch lengths have Nu numbers very close to each other. In the turbulent region, model with 3 mm pitch length gives the highest Nu numbers, while the model with 6 mm pitch length has the lowest Nu numbers. It was noticed that Nu number decreases with growth in pitch length. Decreasing pitch length increases the number of fins and thus enlarges the HT surface area. Increase in HT surface area yields higher Nu numbers. Results demonstrated that using model with 3 mm pitch length increases the Nu number up to 4.8% in the laminar region and up to 7.8% in the turbulent region compared to the model with 4 mm pitch length.

Mohammed et al. [26] studied the influences of geometrical parameters on HT performance inside 10 mm diameter transversely finned tubes for Re number changing from 5000 to 60000. They stated that Nu number increases with decreasing roughness pitch. Aroonrat et al. [25] investigated the impact of pitch length on flow characteristics inside 7.1 mm diameter finned tubes. They reported that Nu number increases with decreasing fin pitch length. Mogaji et al. [29] also observed that decreasing fin pitch length increases the Nu number in their study for 19 mm diameter helically finned tube.

Fig. 10 presents pressure drop and friction factor values of the circular finned tube models with different pitch lengths in laminar and turbulent regions. It was observed that finned tube models have almost identical pressure drop values in laminar region. In turbulent region model with 3 mm pitch length has slightly higher pressure drop values than the other models while, the other models have pressure drop values very close to each other. As expected, all the models have almost identical friction factor values in laminar region. In turbulent region, model with 3 mm pitch length has slightly higher friction factor values than the other models while the model with 6 mm pitch length slightly lower friction factor values compared to other models. Model with 3 mm pitch length has up to 5.34%, 7.81% and 8.66% higher friction factor values compared to the models with 4, 5 and 6 mm pitch length respectively.

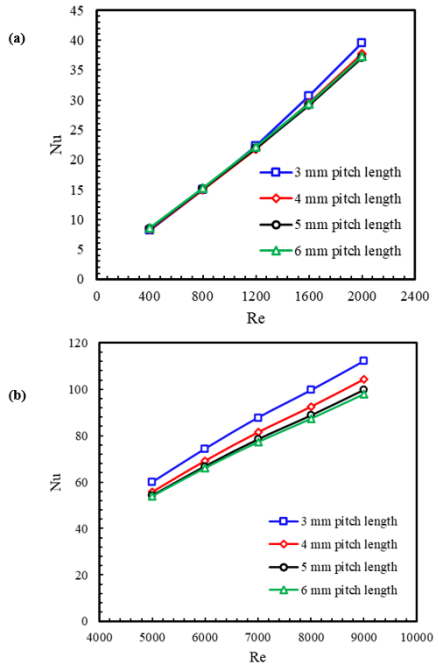

Figure 9. Reynolds number versus Nusselt number plot of circular finned tubes with different pitch lengths for **(a)** laminar and **(b)** turbulent flow

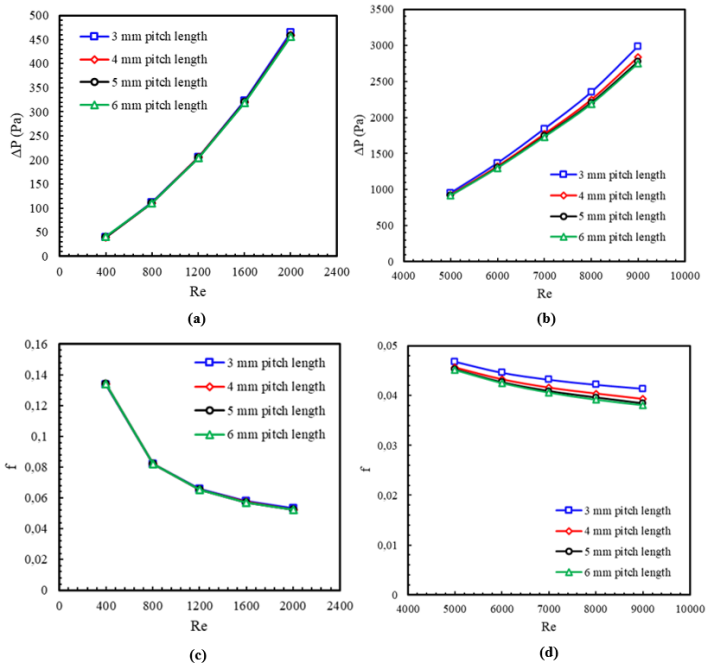

Figure 10. Reynolds number versus pressure drop plot of circular finned tubes for **(a)** laminar and **(b)** turbulent regions; Reynolds number versus friction factor plot of circular finned tubes for **(c)** laminar and **(d)** turbulent flow

In Fig. 11 PEC values of the circular finned tube models with different pitch lengths in laminar and turbulent regions are presented. All the models have PEC values greater than 1 in both laminar and turbulent regions. It was seen that circular finned tube models have identical PEC values Re numbers up to 1200. After the Re number of 1200, model with 3 mm pitch length has higher PEC values compared to the other models. In turbulent region, model with 3 mm pitch length has the highest PEC values among all the models while, model with 6 mm pitch length has smaller PEC values compared to the other models. For circular finned tube model with 3 mm pitch length, PEC values range from 1.12 to 2.79 and 1.26 to 1.33 for laminar and turbulent regions respectively. Results showed that using the model with 3 mm pitch length enhances the PEC value up to 4.4% in the laminar region and up to 6.5% in the turbulent region compared to the model with 4 mm pitch length.

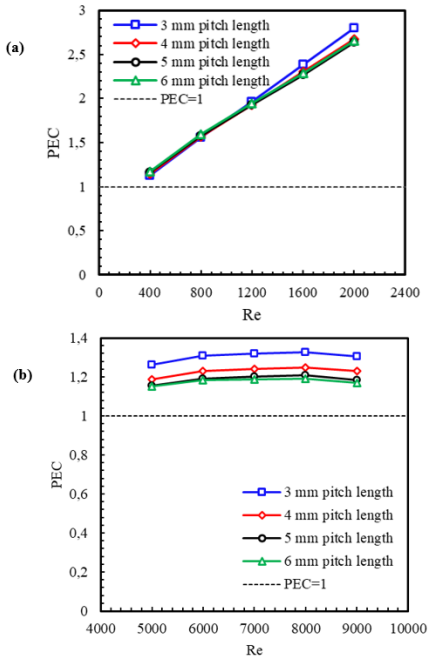

Figure 11. Reynolds number versus PEC plot of circular finned tubes with different pitch lengths for **(a)** laminar and **(b)** turbulent flow

Fig. 12 illustrates the entropy generation ratio of circular finned tubes with different pitch lengths to entropy generation rate of smooth tube for laminar and turbulent regions. As illustrated in Fig. 12, circular finned tube model with 3 mm pitch length has slightly higher entropy generation rate compared to the other circular finned tube models in both laminar and turbulent regions. Moreover, model with 6 mm pitch length possesses the lowest entropy generation rate among all the circular finned tube models. For 3 mm pitch length model, ratio of the entropy generation rate of the circular finned tubes to smooth tube ranges from 0.44 to 1.29 and 1.06 to 1.14 for laminar and turbulent regions respectively. Fig. 12(b)further reveals

that, for all models, the minimum entropy generation ratio occurs at a Re number of 8000. This can be considered an important indicator of the optimal Re number in terms of the entropy generation ratio.

Results demonstrated that Nu number, friction factor and pressure drop tend to increase with declining fin pitch length. The decrease in the fin pitch length leads to an increase in the number of fins and thus more turbulence and disturbance in the flow. This gives rise to an increase in the Nu number as well as in the friction factor and pressure drop. Additionally, increasing HT surface area due to greater number of fins also contributes to the HT augmentation. On the one hand, decreasing the fin pitch length increases the HT performance by providing better fluid mixing and more disturbance in the flow, on the other hand, it raises the pressure loss and thus the friction factor. When both Nu number and friction factor values are taken into account and PEC values are evaluated, results revealed that the circular finned tube model with 3 mm fin pitch length is superior in both turbulent and laminar zones.

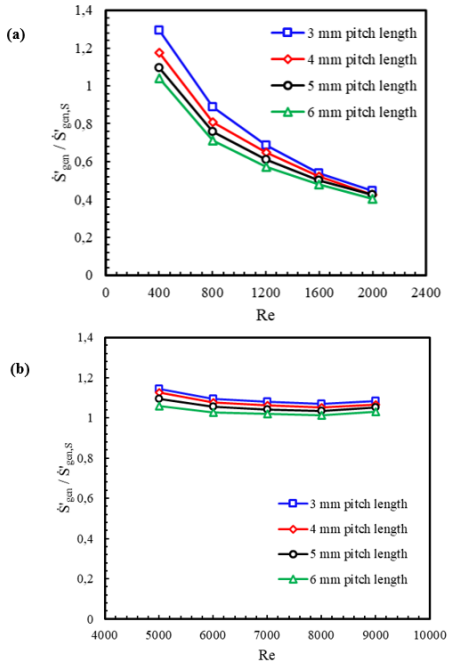

Figure 12. Reynolds number versus ratio of entropy generation rate of circular finned tubes with different pitch lengths to smooth tube plot for **(a)** laminar and **(b)** turbulent flow

4. Conclusion

The demand for smaller yet more powerful electronic devices in various applications results in excess heat that must be effectively dissipated. Therefore, enhancing the heat transfer efficiency of cooling systems is of critical importance. Despite the extensive research on enhanced heat transfer techniques, studies investigating the influence of fin geometry on the thermohydraulic performance of micro-finned tubes remain relatively scarce. Moreover, there are very few studies focusing on entropy generation and performance evaluation criteria (PEC) for tubes with diameters smaller than 10 mm. To address this gap, in this paper, HT and pressure drop characteristics of 8 mm diameter horizontal finned tubes with different finned shapes (circular, square and triangular) numerically investigated using water as working fluid.

Results of this present paper showed that in laminar region, Nu number rises up to 218%, 180% and 140% for circular, triangular and square finned tube respectively compared to smooth tube. In turbulent region, it was seen that Nu number enhances up to 29%, 7.5% and 3.4% for circular, triangular and square finned tube respectively compared to smooth tube. It was revealed that the circular finned tube exhibits the highest Nu numbers in both the laminar and turbulent flow regions among the finned tube models, whereas the square finned tube shows the lowest Nu numbers in both regions. However, circular finned tube has lower pressure drop and friction factor values compared to square and triangular finned tubes in turbulent region among the finned tubes. Besides, PEC values for each finned tube were computed to examine the thermohydraulic performance of finned tubes. It was seen that circular finned tube has the highest PEC values while, square finned tube has the lowest PEC values among the finned tube models. In addition to its higher HT performance, the circular finned tube also yields the lowest entropy generation rate among the finned tube models.

So as to further augment the thermohydraulic performance of circular finned tube, models with different pitch lengths were examined. Besides the circular finned tube model with 4 mm pitch length, additional numerical models with pitch lengths of 3, 5, and 6 mm were numerically investigated. It was seen that model with 3 mm pitch length has higher Nu numbers in both laminar and turbulent regions. It was observed that decreasing pitch length increases Nu number, friction factor and pressure loss in turbulent region. Model with 3 mm pitch length has also higher PEC values compared to other models. Despite its slightly larger friction factor and entropy generation rate, 3 mm pitch length model has greater thermohydraulic performance compared to other circular finned tube models.

While this paper provides valuable insights, it has several limitations that should be acknowledged including limited range of micro fin geometries and flow parameters. Besides, the fluid domain was simplified to a 2D model to minimize computational load.

Copyright and permission statement

All figures presented in this paper were originally created by the authors. No copyrighted images, illustrations, or other visual materials from third-party sources have been used.

Nomenclature

C_p	Specific heat in constant pressure (kJ/kg-K)
C_v	Specific heat in constant volume (kJ/kg-K)

D	Tube diameter (m)
D_h	Hydraulic diameter (m)
D_ω	Cross-diffusion term
E	Total energy (J)
f	Friction factor
f_{app}	Apparent friction factor
f_f	Fanning friction factor
$\widetilde{G_k}$	Generation of turbulence kinetic energy
h	Heat transfer coefficient (W/m^2 K)
k	Turbulence Kinetic Energy (m^2/s^2)
k_{eff}	Effective conductivity (W/m-K)
k_f	Thermal conductivity of fluid (W/m-K)
$K(\infty)$	Incremental pressure drop number
L	Tube length (m)
$\dot{m}$	Mass flow rate (kg/s)
Nu	Nusselt Number
P	Pressure (Pa)
p_l	Pitch length (mm)
Pr	Prandtl Number
q'	Heat transfer rate per unit length (W/m)
q''	Heat flux (kW/m^2)
Re	Reynolds Number
S_k	User-defined source term
S_ω	User-defined source term
$\dot{S}'_{gen}$	Entropy generation (W/m K)
T	Temperature (˚C)
T_{inlet}	Inlet temperature (˚C)
u	Mean velocity (m/s)
u'	Fluctuated velocity component (m/s)
x	Cartesian coordinate along the flow direction (m)
x^*	Dimensionless axial distance (x / D_h Re Pr)
x^+	Dimensionless axial distance (x / D_h Re)
Y_k	Dissipation of k
Y_ω	Dissipation of ω

Greek symbols

Γ_k	Effective diffusivity of ω
Γ_ω	Effective diffusivity of
ε	Turbulent dissipation rate (m^2/s^3)
μ	Dynamic viscosity (Pa-s)
μ_t	Turbulent viscosity (Pa-s)
ν	Kinematic viscosity (m^2/s)
ρ	Density (kg/m^3)
σ_k	Turbulent Prandtl number for k
σ_ω	Turbulent Prandtl number for ω
τ_{eff}	Stress tensor (Pa)
ω	Specific dissipation rate (1/s)
ΔP	Pressure drop (Pa)

Subscripts

gen	Generation
s	Smooth

Conflict of interest

The authors have no conflict of interests to disclose.

Authors contribution

Ahmet Furkan Urkut: Conceptualization, Investigation, Resources, Analysis, Writing (original draft), Validation, Visualization. Mehmed Rafet Özdemir: Conceptualization, Writing (review and editing), Supervision. All authors have read and agreed to the published version of the manuscript.

Ethics

There are no ethical issues with the publication of this manuscript.

References

[1] Fabbri M, Dhir VK. Optimized Heat Transfer for High Power Electronic Cooling Using Arrays of Microjets. Journal of Heat Transfer 2005;127(7):760-769. doi:10.1115/1.1924624.

[2] Sökücü MH, Özdemir MR. Design and implementation of minichannel evaporator for electronics cooling. Journal of Thermal Analysis and Calorimetry 2021;143:3761-3773. doi:10.1007/s10973-020-10457-9.

[3] Urkut AF. Optimization of groove geometry for single phase water flow inside horizontal tubes: a numerical study [MSc thesis]. Marmara University, Istanbul; 2022.

[4] Rashidi S, Hormozi F, Sarafraz MM. Potentials of Boiling Heat Transfer in Advanced Thermal Energy Systems. Journal of Thermal Analysis and Calorimetry 2021;143:1833–1854. doi:10.1007/s10973-020-09511-3.

[5] Karayiannis TG, Mahmoud MM. Flow Boiling in Microchannels: Fundamentals and Applications. Applied Thermal Engineering 2017;115:1372-1397. doi:10.1016/j.applthermaleng.2016.08.063.

[6] Çengel YA. Heat and Mass Transfer: A Practical Approach. 3rd ed. McGraw-Hill;2006.

[7] Liang G, Mudawar I. Review of spray cooling – Part 1: Single-Phase and Nucleate Boiling Regimes, and Critical Heat Flux. International Journal of Heat and Mass Transfer 2017;115:1174-1205. doi:10.1016/j.ijheatmasstransfer.2017.06.029.

[8] Roe C, Feng X, White G, Li R, Wang H, Rui X, Li C, Zhang F, Null V, Parkes M, Patel Y, Wang Y, Wang H, Ouyang M, Offer G, Wu B. Immersion cooling for lithium-ion batteries – A review. Journal of Power Sources 2022;525:231094. doi:10.1016/j.jpowsour.2022.231094.

[9] Özdemir MR, Kaya A, Koşar A. Low mass quality flow boiling in microtubes at high mass fluxes. Journal of Thermal Science and Engineering Applications 2011;3(4):041001. doi:10.1115/1.4005053.

[10] Özdemir, MR, Koşar A. Thermally developing single-phase flows in microtubes. Journal of heat transfer 2013;135(7):074502. doi:10.1115/1.4023881.

[11] Sarkar J. Transcritical CO2 Refrigeration Systems: Comparison with Conventional Solutions and Applications. International Journal of Air-Conditioning and Refrigeration 2012;20:1250017. doi:10.1142/S2010132512500174.

[12] Rony RU, Yang H, Krishnan S, Song J. Recent Advances in Transcritical CO2 (R744) Heat Pump System: A Review. Energies 2019;12(3):457. doi:10.3390/en12030457.

[13] Lorentzen G. Revival of carbon dioxide as a refrigerant. International Journal of Refrigeration 1994;17(5):292-301. doi:10.1016/0140-7007(94)90059-0.

[14] Bolaji BO, Huan Z. Ozone depletion and global warming: Case for the use of natural refrigerant – a review. Renewable and Sustainable Energy Reviews 2013;18:49-54. doi:10.1016/j.rser.2012.10.008

[15] ASHRAE. 15 & 34 Safety Standard for Refrigeration Systems and Designation and Classification of Refrigerants ISO 5149 Mechanical Refrigerating Systems Used for Cooling and Heating—Safety Requirements.

[16] Kharazi AA, Müller N. Comparing water(R718)to other refrigerants. In: Proceedings of the ASME 2006 International Mechanical Engineering Congress and Exposition 2006:85-93. doi:10.1115/IMECE2006-13341.

[17] Kılıçarslan A, Müller N. A comparative study of water as a refrigerant with some current refrigerants. International Journal of Energy Research 2005;29:947–959. doi:10.1002/er.1084.

[18] Bilen K, Cetin M, Gul H, Balta T. The investigation of groove geometry effect on heat transfer for internally grooved tubes. Applied Thermal Engineering 2009;29(4):753-761. doi:10.1016/j.applthermaleng.2008.04.008.

[19] Selvaraj P, Sarangan J, Suresh S. Experimental Investigation on Heat Transfer and Friction Factor Characteristics of a Water and Ethylene Glycol Mixture Flow of Internally Grooved Tubes. International Journal of Chemical Research 2011;3(1):33-40.

[20] Pethkool S, Eiamsa-ard S, Kwankaomeng S, Promvonge P. Turbulent heat transfer enhancement in a heat exchanger using helically corrugated tube. International Communications in Heat and Mass Transfer 2011;38(3):340-347. doi:10.1016/j.icheatmasstransfer.2010.11.014.

[21] Inoue N, Ichinose J. Single-Phase Heat Transfer And Pressure Drop Inside Internally Helical-Grooved Horizontal Small-Diameter Tubes. International Journal of Air-Conditioning and Refrigeration 2012;20:1250022. doi:10.1142/S2010132512500228.

[22] Celen A, Dalkilic AS, Wongwises S. Experimental analysis of the single phase pressure drop characteristics of smooth and microfin tubes. International Communications in Heat and Mass Transfer 2013;46:58-66. doi:10.1016/j.icheatmasstransfer.2013.05.010.

[23] Selvaraj P, Sarangan J, Suresh S. Computational fluid dynamics analysis on heat transfer and friction factor characteristics of a turbulent flow for internally grooved tubes. Thermal Science 2013;17(4):1125-1137. doi:10.2298/TSCI110404010S.

[24] Ramadhan AA, Al Ani YT, Shareef AJ. Groove geometry effects on turbulent heat transfer and fluid flow. Heat and Mass Transfer 2013;49:185–195. doi:10.1007/s00231-012-1076-9.

[25] Aroonrat K, Jumpholkul C, Leelaprachakul R, Dalkilic AS, Mahian O, Wongwises S. Heat transfer and single-phase flow in internally grooved tubes. International Communications in Heat and Mass Transfer 2013;42:62-68. doi:10.1016/j.icheatmasstransfer.2012.12.001.

[26] Mohammed HA, Abbas AK, Sheriff JM. Influence of geometrical parameters and forced convective heat transfer in transversely corrugated circular tubes. International Communications in Heat and Mass Transfer 2013;44:116-126. doi:10.1016/j.icheatmasstransfer.2013.02.005.

[27] Wang YH, Zhang JL, Ma ZX. Experimental determination of single-phase pressure drop and heat transfer in a horizontal internal helically-finned tube. International Journal of Heat and Mass Transfer 2017;104:240-246. doi:10.1016/j.ijheatmasstransfer.2016.08.045.

[28] Kaood A, Abou-Deif T, Eltahan H, Yehia MA, Khalil EE. Numerical investigation of heat transfer and friction characteristics for turbulent flow in various corrugated tubes. Proceedings of the Institution of Mechanical Engineers, Part A: Journal of Power and Energy 2019;233(4):457-475. doi:10.1177/095765091880640.

[29] Mogaji TS, Olapojoye AO, Idowu ET, Saleh B. CFD study of heat transfer augmentation and fluid flow characteristics of turbulent flow inside helically grooved tubes. Journal of the Brazilian Society of Mechanical Sciences and Engineering, 2022;40:90. doi:10.1007/s40430-021-03299-5.

[30] Khudheyer AF, Al-Abbas AH, Carutasiu MB, Necula H. Turbulent heat transfer for internal flow of ethylene glycol-al2o3 nanofluid in a spiral grooved tube with twisted tape inserts. Journal of Thermal Engineering 2021;*7*(4):761-772. doi:10.18186/thermal.928556

[31] Wu G, Wang E, Xu J, Wang H. Investigation on heat transfer enhancement performance of helical micro-grooved tubes: comparative analysis and optimization of micro-groove structures. Thermal Science and Engineering Progress, 2025;64:103778. doi:10.1016/j.tsep.2025.103778

[32] Sharifzadeh R, Mahdizadeh M, Afshari A. Investigating swirling flow effects on thermo-fluid characteristics of a grooved pipe heat exchanger. International Communications in Heat and Mass Transfer, 2025;168:109417. doi:10.1016/j.icheatmasstransfer.2025.109417ANSYS FLUENT 14.0. Theory Guide; 2011.

[33] Incropera FP, De Witt DP. Fundamentals of Heat and Mass Transfer, 5th ed. New York: John Wiley and Sons; 2002.

[34] Hellsten A, Laine S. Extension of the k-omega-SST turbulence model for flows over rough surfaces. In: Proceedings of the 22nd Atmospheric Flight Mechanics Conference. AIAA Paper 1997-3577. Reston, VA: American Institute of Aeronautics and Astronautics; 1997. doi:10.2514/6.1997-3577

[35] Yangaz MU, Özdemir MR, Şener R. Combustion performance of hydrogen-enriched fuels in a premixed burner. Environmental technology 2020;41(1): 2-13. doi:10.1080/09593330.2019.1656676.

[36] Menter FR. Two-Equation Eddy-Viscosity Turbulence Models for Engineering Applications. AIAA journal 1994;32:1598-1605.

[37] ANSYS Fluent 15.0. User's Guide; 2013.

[38] Di Piazza I, Ciofalo M. Numerical prediction of turbulent flow and heat transfer in helically coiled pipes. International Journal of Thermal Sciences 2010;49(4):653-663. doi:10.1016/j.ijthermalsci.2009.10.001.

[39] Sparrow EM, Tong JC, Abraham JP. Fluid Flow in a System with Separate Laminar and Turbulent Zones. Numerical Heat Transfer, Part A: Applications 2008;53:341-353. doi:10.1080/10407780701454162.

[40] Singh V, Chamoli S, Kumar M, Kumar A. Heat transfer and fluid flow characteristics of heat exchanger tube with multiple twisted tapes and solid rings inserts. Chemical Engineering and Processing: Process Intensification 2016;102:156-168. doi:10.1016/j.cep.2016.01.013.

[41] Wang W, Zhang Y, Li Y, Han H, Li B. Multi-objective optimization of turbulent heat transfer flow in novel outward helically corrugated tubes. Applied Thermal Engineering 2018;138:795-806. doi:10.1016/j.applthermaleng.2017.12.080.

[42] Bejan A. Entropy Generation Minimization: The Method of Thermodynamic Optimization of Finite-Size Systems and Finite-Time Processes. CRC Press; 1996.

[43] Hong SH, Hrnjak PS. Heat transfer in thermally developing flow of fluids with high Prandtl numbers preceding and following U-bend. Urbana, IL: Air Conditioning and Refrigerating Center, University of Illinois; 1999.

[44] Shah RK, Sekulić DP. Fundamentals of Heat Exchanger Design. John Wiley & Sons; 2003.

[45] [46] Shah RK, London AL. Laminar Flow Forced Convection in Ducts. New York: Academic Press;1978.

[46] Dittus FW, Boelter LMK. Heat transfer in automobile radiators of the tubular type. Publications in Engineering 1930;2:443-461.

[47] Gnielinski V. New equations for heat and mass transfer in turbulent pipe and channel flow. International Chemical Engineering 1976;16(2):359-368.

[48] Blasius H. Das Ähnlichkeitsgesetz bei Reibungsvorgängen in Flüssigkeiten. In: Mitteilungen über Forschungsarbeiten auf dem Gebiete des Ingenieurwesens. Berlin, Heidelberg: Springer; 1913.

[49] Xu X, Zhang Y, Liu C, Zhang S, Dang C. Experimental investigation of heat transfer of supercritical CO2 cooled in helically coiled tubes based on exergy analysis. International Journal of Refrigeration 2018;89:177-185. doi:10.1016/j.ijrefrig.2018.03.011.

[50] Chaware P, Sewatkar CM. Effects of tangential and radial velocity on fluid flow and heat transfer for flow through a pipe with twisted tape insert—laminar flow. Sādhanā 2018;43:150. doi:10.1007/s12046-018-0893-z.